J Mater Sci

Electronic materials

Characterization of flexible low-dielectric constant carbon-doped oxide (SiCOH) thin films under repeated mechanical bending stress

William Wirth[1], Jacob Comeaux[1], and Seonhee Jang[1,*]

[1] *Department of Mechanical Engineering, University of Louisiana at Lafayette, Lafayette, LA 70503, USA*

Received: 30 September 2022
Accepted: 16 November 2022

ABSTRACT

Flexible low-dielectric constant (low-k, $k < 4.0$) SiCOH films were deposited onto ITO/PEN flexible substrates by plasma-enhanced chemical vapor deposition of tetrakis(trimethylsilyloxy)silane precursor at room temperature with plasma powers from 20 to 100 W. The pristine SiCOH films had a mechanical strength up to 9.1 GPa and a low k-value down to 2.00, and they were transparent, smooth, and hydrophobic. As the plasma power increased, there were an increase in the suboxide structure, increase in density, and decrease in the methyl group concentration. In the lower plasma power regime of 20–60 W, the k-value decreased as the plasma power increased due to the increased suboxide structure. In the higher plasma power regime of 60–100 W, the k-value increased as the plasma power increased due to the decreased methyl concentration and increased density. The mechanical properties increased as the plasma power increased. Upon repeated mechanical bending tests with bending cycles up to 10,000, the flexible SiCOH films maintained their transparency, smoothness, and hydrophobicity and showed a stable k-value below 4.0. There were no significant changes in the FTIR spectra and no cracks or delamination observed in the films. The SiCOH films showed stable physical, chemical, and electrical properties under the repeated mechanical bending.

Introduction

The microelectronics and semiconductor industries continue to push the boundaries of materials science. One specific example is the continued progress of increasing transistor density for integrated circuit (IC) chips. The industry has been motivated to follow the idea set by Moore's law [1]. These chips are made by two encompassing processes called the front end of line (FEOL) and back end of line (BEOL). The FEOL manufacturing process creates the functional

Handling Editor: Kevin Jones.

Address correspondence to E-mail: seonhee.jang@louisiana.edu

https://doi.org/10.1007/s10853-022-07987-y

Published online: 27 November 2022

components of the IC chip, such as transistors. The metal lines and vias connect the functional devices within the FEOL to each other. The interlayer dielectrics surround the metal lines and vias for both the local and global interconnects. The purpose of the interconnect structure is to use the metal lines and vias to conduct electrical signals from one transistor to another through the local interconnect, and vertically to the contact pads external to the IC chip. The BEOL structure can be a limiting factor on the performance of an IC chip due to the resistance-capacitance (RC) delay. An increased RC delay reduces the effective speed of an IC chip [2]. The RC delay for an interconnect structure is calculated by an equation $RC = 2\rho k\varepsilon_0\left(\frac{4L^2}{P^2} + \frac{L^2}{T^2}\right)$, where ε_0 is the vacuum permittivity, ρ is resistivity of the metal line, and k is the relative dielectric constant of the dielectric material [3]. RC delay also depends on geometry, where L is the metal line length, P is the metal pitch, and T is the dielectric thickness. As IC chip features scale down to increase the transistor density, both L/P and L/T ratios increase, resulting in an increased RC delay. Therefore, in order to reduce the RC delay, both the resistivity and dielectric constant must be reduced.

Traditionally, aluminum (Al) and silicon oxide (SiO_2) were utilized for the metal and dielectric materials for interconnects, respectively. The industry had replaced aluminum (2.6×10^{-8} Ω·m) with the lower resistivity copper (Cu, 1.7×10^{-8} Ω·m) in the late 1990s [4–6]. Next, the industry replaced SiO_2 (k = 4.2) dielectrics with low dielectric constant (low-k, $k < 3.5$) SiCOH [5]. Another benefit of utilizing low-k materials for interconnects is the reduced power consumption. The relationship between the capacitance and power consumption (P) can be expressed by an equation, $P = CV^2f$, where C is the capacitance, V is the operating voltage, and f is the operating frequency [5]. A lower dielectric constant results in a lower capacitance and therefore lower power consumption.

On the other hand, the microelectronics and semiconductor industries are also increasing research on flexible electronics [7, 8]. These are different from the traditional rigid electronics that are developed on silicon (Si) wafers. Flexible electronics typically utilize polymer substrates that allow bending or stretching of the electronic device, which drastically expands its applications. This technology has proven to be useful in industry and research to create flexible displays, wearable devices, and flexible solar cells [9–12]. One of the materials utilized by thin film transistors (TFT) devices is flexible dielectric films [7, 8]. It has been reported that the flexible dielectric films with high dielectric constants ($k > 3.9$) can be used to improve gate performance of TFTs fabricated on flexible substrates [7]. However, few reports have been found in development of flexible dielectric films with low dielectric constant ($k < 3.9$) fabricated on flexible substrates. Some applications of flexible materials have additional requirements. For example, transparency is often required for flexible displays. Polymers typically have low glass transition temperatures, making them susceptible to damage from elevated temperatures. For example, polyethylene naphthalate (PEN) has a glass transition temperature of 120 °C [13]. This limits the process temperature below 120 °C in order to prevent the glass transition of the PEN polymer substrate. Using polymer substrates for flexible electronics requires process temperature as low as possible.

In this study, flexible low-k SiCOH films were prepared by plasma-enhanced chemical vapor deposition (PECVD) of a single precursor of tetrakis(trimethylsilyloxy)silane (TTMSS, $C_{12}H_{36}O_4Si_5$) at different plasma deposition conditions, yielding the films with varying material properties. Physical properties including refractive index, extinction coefficient, morphology and roughness, and contact angle were analyzed. Chemical structures and elemental composition were studied. One of the electrical properties, dielectric constant, was correlated with physical and chemical properties. Elastic modulus and hardness were measured to study mechanical properties. The pristine SiCOH thin films were then used for bending tests up to 10,000 bending cycles. Characterization of physical, chemical, and electrical properties after bending tests was conducted to determine any effect on the SiCOH films. Altogether, this research aims to characterize SiCOH films and determine the applicability of such films for flexible electronics by observing the effects of repeated mechanical bending tests.

Experimental details

Flexible SiCOH thin films were deposited onto flexible ITO/PEN (indium tin oxide/polyethylene naphthalate) substrates by the PECVD process of the

TTMSS (Sigma Aldrich, 97% purity) precursor. Figure 1 shows the molecular structure of the TTMSS precursor. The molecule is composed of silicon (Si), carbon (C), oxygen (O), and hydrogen (H). The molecular formula is $C_{12}H_{36}O_4Si_5$. The structure is centered on a single Si atom with four oxygen atoms covalently bonded. Each of these oxygen atoms covalently bonds to another Si atom. Branching off each Si atom is three methyl groups (CH_3). The important characteristics of this bonding structure are the Si–O–Si bonds at the center of the molecule and the many methyl groups branching off.

The flexible ITO-coated PEN substrate purchased from MTI corporation had thicknesses of 180 μm and 125 μm for ITO and PEN, respectively. The PEN substrate was DuPont Teijin Teonex film-Q65HA. The ITO coating method was magnetron sputtering. A resistance was 12 Ω/square, and a transparency was greater than 75%. The ITO layer of the substrate was initially protected by a protective film to prevent contamination on the surface. The protective film was removed before the substrate was loaded for the deposition. A radio frequency (RF) power with 13.56 MHz supplied PECVD system was used. The deposition process occurred inside the reactor chamber. A susceptor was located at the bottom of the reactor and acted as a platform to hold the substrate. A shower head was located at the top of the reactor. The distance between the susceptor and the shower head was 20 mm. There was a bubbler containing the organic precursor. There were an inlet and an outlet of the bubbler. A gas line from the Ar gas cylinder containing Ar gas with a purity of 99.999% was connected to inlet of the bubbler. The outlet of the bubbler was connected to the shower head of the PECVD reactor via the gas line. Ar gas flew into the heated bubbler through the inlet, and vapors of the organic precursor were produced at the elevated temperature. The vaporized precursor was delivered to the shower head through the outlet of the bubbler. Ar gas acted as a carrier gas and transferred the vapors down the line connected to the reactor. The mixture flows with the vaporized precursor carried by Ar gas flew into the reactor via the shower head. The other input was a simple Ar line fed into the shower head. The second Ar input line was not necessary for deposition, but it was utilized in Ar plasma generation only. The flow of precursor vapors was controlled by a mass flow controller (MFC) and a pressure flow controller (PFC). The MFC was located between the Ar gas cylinder and the inlet of the bubbler and the PFC between the outlet of the bubbler and the reactor. At the bottom of the reactor, there was a vacuum line leading to the dry screw pump. When the substrate was loaded on the susceptor, the pump lowered the reactor pressure to a rough vacuum range about 0.133 Pa, which was a base pressure prior to deposition. When the reactor pressure reached to the base pressure, Ar gas was introduced to the reactor through the second Ar input line. This Ar line was controlled by another MFC. With a flow rate of 50 sccm, an Ar plasma was generated at 50 W for 3 min to activate the substrate. After Ar plasma, the deposition of SiCOH thin film was conducted. To vaporize the liquid precursor effectively, the bubbler containing the TTMSS precursor was heated to 85 °C. Ar gas was then used as the carrier gas which transported the vaporized precursor from the bubbler to the reactor. The films were deposited at room temperature at an operating pressure of 26.7 Pa. The flow rate of Ar gas flowing through the bubbler was maintained at 18 sccm via the MFC. The pressure flow of vaporized precursor into the reactor was maintained at 30 Torr via the PFC. The RF plasma power with 13.56 MHz was chosen in the range of 20–100 W. A deposition time was fixed at 20 min for all films. Each deposition rate was calculated by the average film thickness divided by the deposition time of 20 min. While these PECVD low-dielectric constant materials are known by many names, including SiCOH, SiOCH, SiOC, carbon-

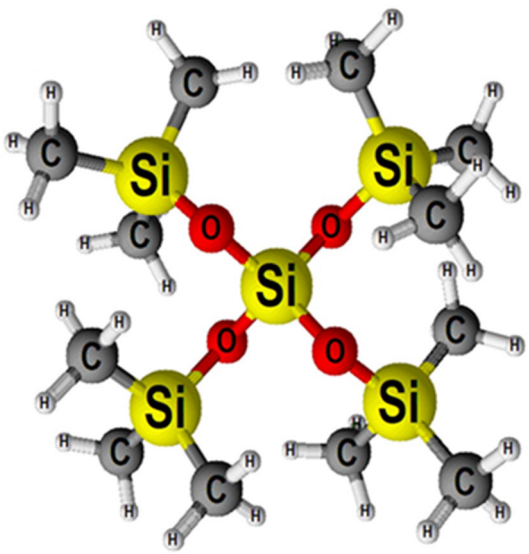

Figure 1 Molecular structure of the TTMSS precursor.

doped oxides, silicon-oxicarbides, and organosilicate glasses, the term SiCOH has been generally revealed in many research papers. The SiCOH is elementally descriptive with four elements of Si, C, O, and H, but not representing the stoichiometry.

The flexible SiCOH thin films were then subjected to repeated mechanical bending. The films at the deposition plasma powers of 20, 60, and 100 W were chosen for repeated mechanical bending tests. These films were represented as the low, medium, and high range of the plasma powers utilized for deposition. The films were prepared for a specific size of 2.5 cm width by 5 cm length. Figure 2a shows a schematic diagram of the device from the top view. There is a rectangular frame that all the components were attached to. The main functionality of this device comes from the precisely machined lead screw that is rotated by a brushless DC motor. A connector nut is on the lead screw and attaches to the mobile holder. The ends of the mobile holder are connected to a track in the frame. This setup creates a translating motion of the mobile holder when the motor turns. Bearing mounts hold the lead screw to the frame, while still allowing free rotation. The stationary holder is fixed to the frame. The distance travelled by the mobile holder is determined by the angle rotated by the motor and the pitch of the lead screw. The motor is controlled by a motor controller. The job of the motor controller is to adjust the power supplied to the motor in order to achieve a desired angular position, velocity, and acceleration. The computer sends the desired angular position, velocity, and acceleration information to the motor controller. Figure 2b–d shows the range of motion achievable for the flexible film. An unstressed film is shown in Fig. 2b. After the film was loaded into the holder, the spacing was slightly decreased to be smaller than the film length as shown in Fig. 2c. At this point, the film was in the extended position. Next, the film was at the bending position, where the spacing was significantly closer than the extended position as shown in Fig. 2d. During one cycle of the repeated mechanical

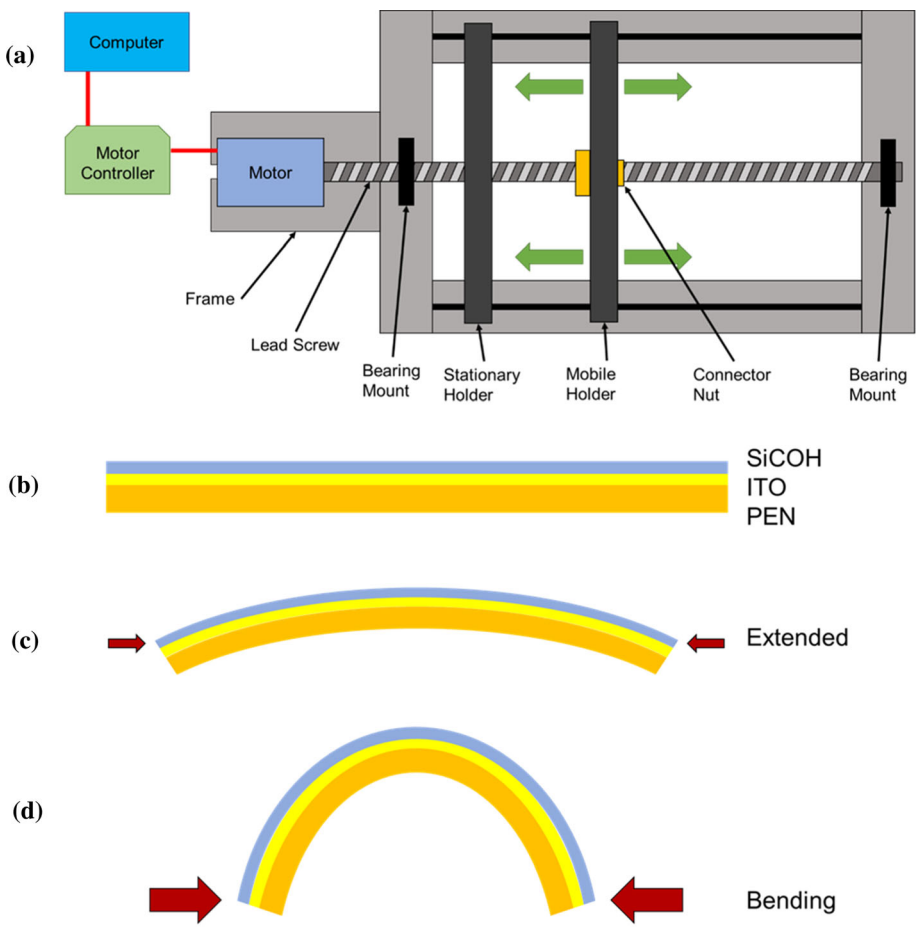

Figure 2 **a** Schematic diagram of the repeated mechanical bending tester and the range of motion for the flexible film including **b** an unstressed film, **c** the extended position, and **d** the bending position for repeated mechanical bending tester.

bending test, the holder position moved from the extended position to the bending position and returned to the extended position at the end of the cycle. The amount of time to complete this cycle was called the period. The film was compressed for the entirety of the cycle in order to keep the film in the holders, even in the extended position. During the bending cycles, the holder spacing was positioned to 4.5 cm for the extended position and 3 cm for the bending position. This achieved a bending radius of 13 mm at the bending position. The bending cycle period was set to 3 s. Bending cycles were applied with 1000, 5000, and 10,000 for each bending test. After the repeated mechanical bending tests were completed, the films were characterized to investigate the change in material properties after bending.

Spectroscopic ellipsometry (RC2, JA Woolman) was utilized to measure the thickness, refractive index, and extinction coefficient of the SiCOH films. Measurements were collected in reflection mode at the angles of 50, 60, and 70 degrees over the range of 210–2500 nm. The refractive index and extinction coefficient were determined by extrapolating the model to 633 nm, which is the typical wavelength value chosen for refractive index comparison. The contact angle was measured by a contact angle goniometer (L2004A, Ossila). Both surface roughness and topology were measured by atomic force microscopy (SmartSPM, Horiba) over a 1 μm by 1 μm area. Scanning electron microscopy (SEM, S-4500 II Cold Field Emission, Hitachi) was utilized to examine any microstructure defects or deformation on the surface of the film after mechanical bending tests. Chemical surface analysis was performed by both X-ray photoelectron spectroscopy (XPS, ESCA 2SR, Scienta Omicron) and Fourier transform infrared (FTIR) spectroscopy (Invenio S, Bruker). XPS survey scans were collected over the range of 0 to 1200 eV at a step of 0.1 eV. Higher-resolution scans were collected with a step of 0.05 eV for individual elemental peak. The samples were sputtered by Ar ions before XPS measurements in order to remove any carbon contamination at the film surface. The electron emission angle was 90° and the diameter of the circular analysis area was 1.93 mm. FTIR spectroscopy collected absorption spectra from 650 to 4000 cm^{-1} with a resolution of 4 cm^{-1}. Al dots were deposited onto the SiCOH film using an evaporation method to create a metal–insulator–metal (MIM) structure (Al/SiCOH/ITO). Al dots were composed of two areas of 0.005288 and 0.008093 cm^2 with a thickness of 120 nm. The spacing between the dots was 0.5 mm. Capacitance–voltage curves were measured over the MIM structure using an LCR meter (J4287A, Agilent). Dielectric constant was calculated by using the formula, $C = \frac{k\varepsilon_0 A}{d}$, where C is the capacitance measured, k is the dielectric constant of the SiCOH thin film, ε_0 is the vacuum permittivity (8.854×10^{-12} F/m), A is an area of the electrodes, and d is a thickness of the SiCOH film. Mechanical properties were measured by nanoindentation (G200 Nano Indenter, KLA) in continuous stiffness measurement (CSM) mode. The elastic modulus and hardness were averaged over 10–15% of the SiCOH film thickness to avoid the influence of the substrate [14, 15]. Sixteen indentations were performed for each sample.

Results and discussion

Figure 3 a–d presents deposition rate, refractive index, extinction coefficient, and contact angle of the pristine flexible SiCOH films at various deposition plasma powers of 20–100 W, respectively. The deposition rate was calculated from the film thickness divided by the deposition time. The deposition rate increased from 26.56 nm/min at 20 W to 40.89 nm/min at 80 W. Then, at a higher plasma power of 100 W, the deposition rate decreased to 30.4 nm/min. This behavior suggested that there was a deposition regime transition at 80 W. It was known that the deposition of the SiCOH films is controlled by the competition between ablation and polymerization mechanisms during plasma polymerization [16]. Two processes occur simultaneously: ablation that removes the surface molecules and polymerization that deposits the surface monomers. These two processes are in competition and the deposition rate could increase or decrease depending on the dominant process. For example, the deposition rate increased when polymerization is preferred. It was likely that the dominant process shifted from polymerization to ablation at 80 W. The refractive index increased from 1.44 to 1.54 as the deposition power increased from 20 to 100 W. The increase in refractive index suggests an increase in the film density. The increase in refractive index from 80 to 100 W was significantly greater than the increase at lower plasma powers. This supported that the transition to

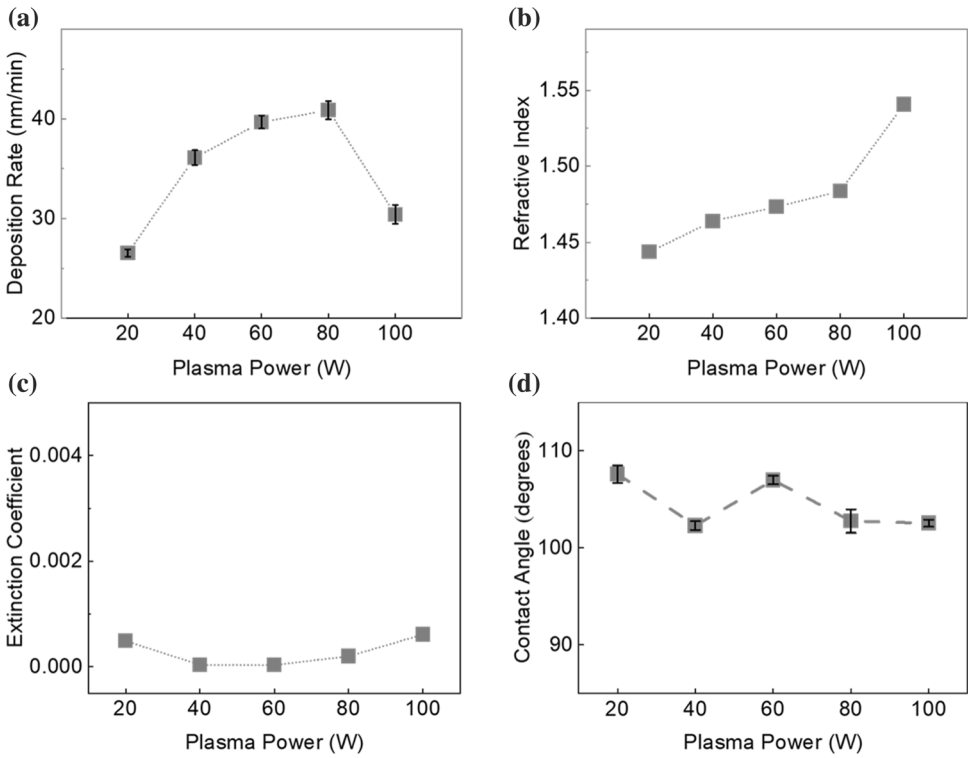

Figure 3 **a** Deposition rate, **b** refractive index, **c** extinction coefficient, and **d** contact angle of the pristine flexible SiCOH films at various deposition plasma powers of 20–100 W.

the higher refractive index above 1.50 occurred at 80 W, as observed in the deposition regime transition at the same plasma power. The extinction coefficient decreased from 0.00049 at 20 W to the smallest value of 0.00003 at 60 W and then increased again to 0.00061 at 100 W. These low extinction coefficient values reflected the transparent nature of the SiCOH films. It is generally admitted that the material having its extinction coefficient below 0.01 is transparent. All SiCOH films with deposition conditions including plasma powers of 20–100 W showed very low extinction coefficients well below 0.01. Apparently, they were all transparent. This transparency was also confirmed by visual inspection. To obtain low extinction coefficient values is important for flexible device applications. The contact angle slightly decreased from 107.61° to 102.52° as the plasma power increased from 20 to 100 W. A hydrophobic material is defined as having a contact angle greater than 90°. Therefore, all SiCOH films were hydrophobic. However, the lower contact angle at the higher plasma power indicated a less hydrophobic film. The hydrophobicity of the film could be related to chemical bonding configurations of the film surface.

Figure 4a presents the RMS surface roughness of the pristine flexible SiCOH thin films at various deposition plasma powers of 20–100 W. All surface roughness values were measured below 2 nm, which was quite small compared to the film's thickness in the range of 500–1200 nm. The surface roughness increased from 0.34 nm at 20 W to the highest roughness value of 1.67 nm at 60 W and then slightly decreased to 1.33 nm at 100 W. This behavior further supported the deposition regime transition, but suggested the transition was between 60 and 80 W. From observations of deposition rate, refractive index, and surface roughness, it was likely that there was transition in physical properties occurring at 60–80 W. Figure 4b–f shows the surface morphology images of the SiCOH films at the deposition plasma powers of 20, 40, 60, 80, and 100 W, respectively. These images illustrated the significantly lower roughness at 20 W compared to the roughness of the higher deposition plasma powers, consistent with RMS roughness in Fig. 4a.

Figure 5a presents the XPS survey scans of the pristine flexible SiCOH films at various deposition plasma powers ranging from 20 to 100 W. The major peaks were identified as the Si2*p*, C1*s*, and O1*s* peaks with peak centers of ~ 102, 285, and ~ 533 eV, respectively [17–19]. High resolution scans for the major peaks allowed measurement of the peak area and therefore the calculation of the atomic

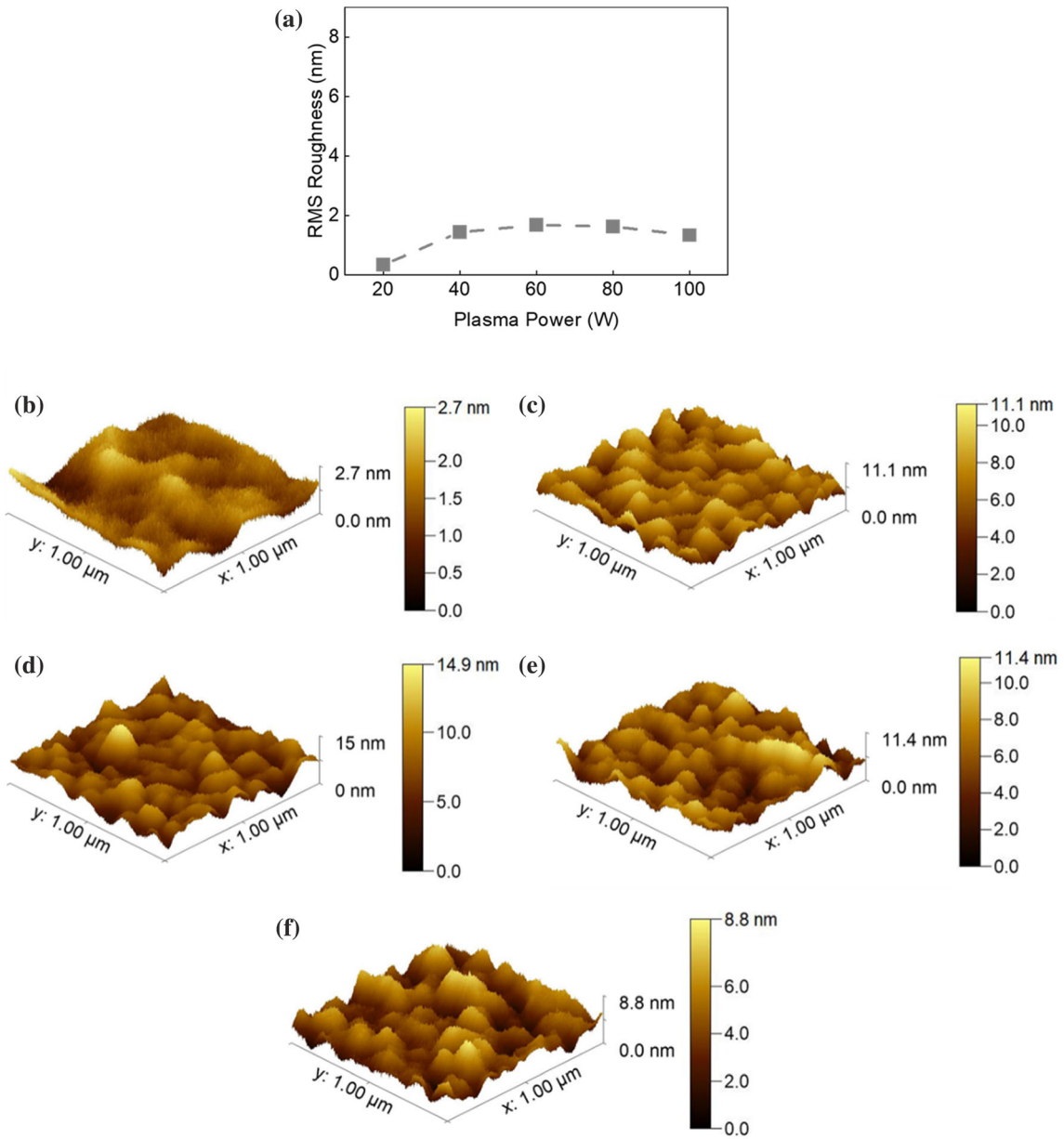

Figure 4 **a** RMS roughness and surface morphology of the pristine flexible SiCOH films at various deposition plasma powers of **b** 20, **c** 40, **d** 60, **e** 80, and **f** 100 W.

concentrations of silicon, carbon, and oxygen. The Si2s peak was also identified at ~ 150 eV with a small intensity. Another peak identified was the O KLL peak at ~ 980 eV, which is a result of the excitation of Auger electron emissions from oxygen. Figure 5b shows the atomic concentrations of the SiCOH films at various deposition plasma powers of 20–100 W. The SiCOH films were high in carbon and silicon, about 40% each. Both the carbon and silicon concentrations slightly decreased as the deposition plasma power increased from 20 to 100 W. A decrease in the carbon concentration has been related to a loss of methyl groups and thus an increase in the dielectric constant in previous studies [20]. The oxygen concentration was low, around 20%, and slightly increased as the deposition plasma power increased from 20 to 100 W.

High-resolution scans allowed further analysis of the Si2*p* and C1*s* peaks. Figure 6a shows an overlay of Si2*p* peaks for 20–100 W. Figure 6b shows an

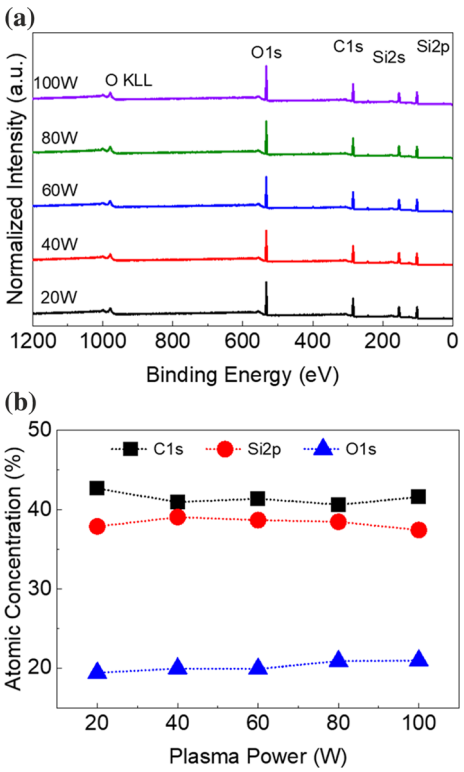

Figure 5 **a** XPS survey scans, **b** atomic concentrations of the pristine flexible SiCOH films at various deposition plasma powers of 20–100 W.

example of the deconvoluted Si2*p* peak for the film at 20 W. The deconvoluted peaks were O–Si–C_3, O_2–Si–C_2, and O_3–Si–C centered at 101.1, 102.0, and 102.9 eV, respectively [18, 21]. These peaks were labeled as M-group, D-group, and T-group, respectively, referring to the number of O atoms bonded to the Si atom. Figure 6c displays the peak area ratios for the three deconvoluted peaks at various plasma powers. The M-group accounted for the smallest peak area ratio, around 13%, and was not significantly affected by the increased plasma power. This indicated high dissociation of the methyl groups from the TTMSS precursor, allowing the formation of the D- and T-groups. For the film at 20 W, the T-group held the largest peak area ratio of 45%, with the D-group just below at 42%. As the plasma power increased from 20 to 100 W, there was a decrease in the T-group, and an increase in the D-group. For the film at 100 W, the D-group was dominant at 62%, while the T-group was at 23%. The D-group promoted chain linking instead of crosslinking like the T-group structure did [17, 18].

An overlay of the C1*s* peak at various deposition plasma powers is shown in Fig. 7a. This illustrated that the film at 20 W had a slightly higher intensity than other films. Deconvolution was performed on the C1*s* peak, and an example of deconvoluted C1*s* peak for the film at 20 W is shown in Fig. 7b. The deconvoluted peaks were identified as C–Si, C–C/C–H, and C–O at the binding energies of 284.0, 284.8, and 287.8 eV, respectively [17–19, 21, 22]. Their respective peak area ratios are shown in Fig. 7c. The largest peak was C–C/C–H with a peak area ratio in the range of 79 to 91%. The smaller peaks of C–O and C–Si both ranged between 4 and 11%. The chemical structure of the TTMSS precursor could be related to these results. TTMSS has more C–H bonds than Si–C bonds, due to the structure of the methyl groups. Therefore, the decrease in carbon concentration is related to decrease in the methyl groups present in the TTMSS precursor. The small amount of C–O indicated that some of the dissociated species allowed recombination to produce them.

Figure 8 shows the full scans of the FTIR spectra for the pristine flexible SiCOH films at various deposition plasma powers of 20–100 W. The major absorption bands were identified as νCHx stretching ranging from 3100 to 2800 cm^{-1}, δSi–CH_3 bending from 1300 to 1200 cm^{-1}, νSi–O–Si stretching from 1200 to 950 cm^{-1}, and νSi–$(CH_3)_x$ stretching from 950 to 650 cm^{-1} [20, 23]. A decrease in peak intensity was observed for the $νCH_x$ and δSi–CH_3 bands as the plasma power increased from 20 to 100 W. This indicated a decrease in methyl groups present in the SiCOH films. Both the νSi–O–Si and νSi–$(CH_3)_x$ bands became narrower as the plasma power increased from 20 to 100 W. This suggested that the films experienced a preference for certain bonding configurations. Deconvolution and closer inspection of these absorption bands provide more details on the chemical bonds of the SiCOH films.

The major absorption band νSi–O–Si was further investigated. Figure 9a presents the overlay of all νSi–O–Si absorption bands at various plasma powers. As the plasma power increased from 20 to 100 W, the peak center shifted from 1030 cm^{-1} to the lower wavenumber of 1015 cm^{-1}. In addition, the shoulder at 1065 cm^{-1} reduced significantly. This indicated that the SiCOH films experienced a preference for the peak at the lower wavenumber as the plasma power increased from 20 to 100 W. Deconvolution was performed on the Si–O–Si stretching band in order to

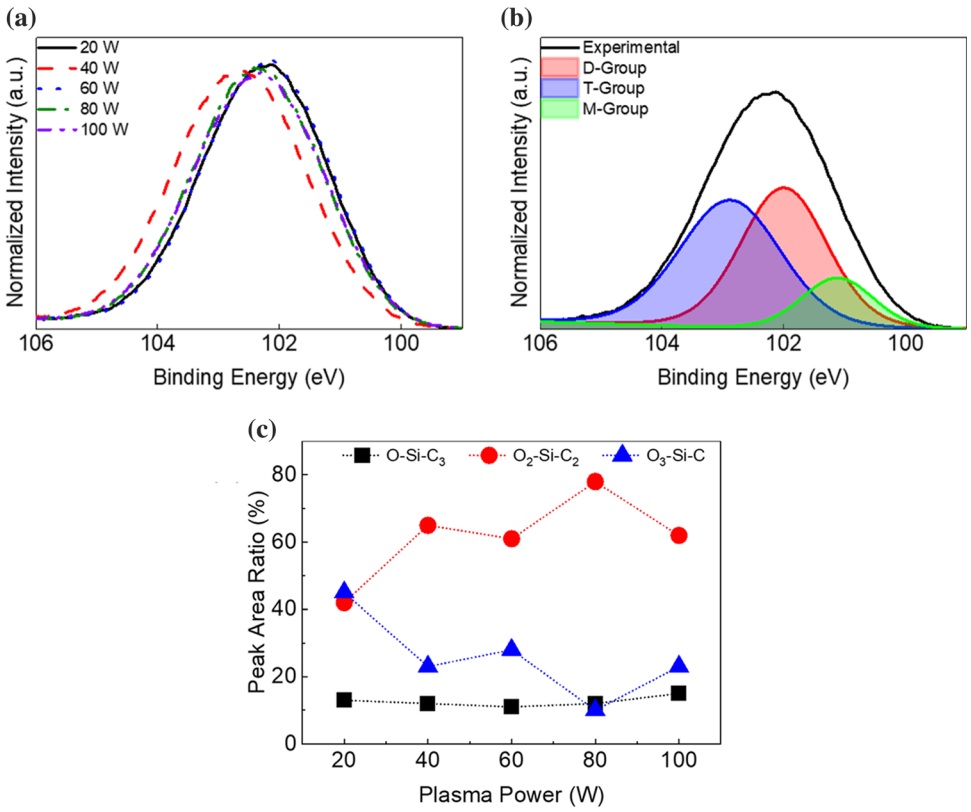

Figure 6 **a** XPS Si2*p* peaks of the pristine flexible SiCOH films at various deposition plasma powers of 20–100 W, **b** deconvoluted Si2*p* peak for 20 W, and **c** peak area ratios of silicon bonds at various plasma powers.

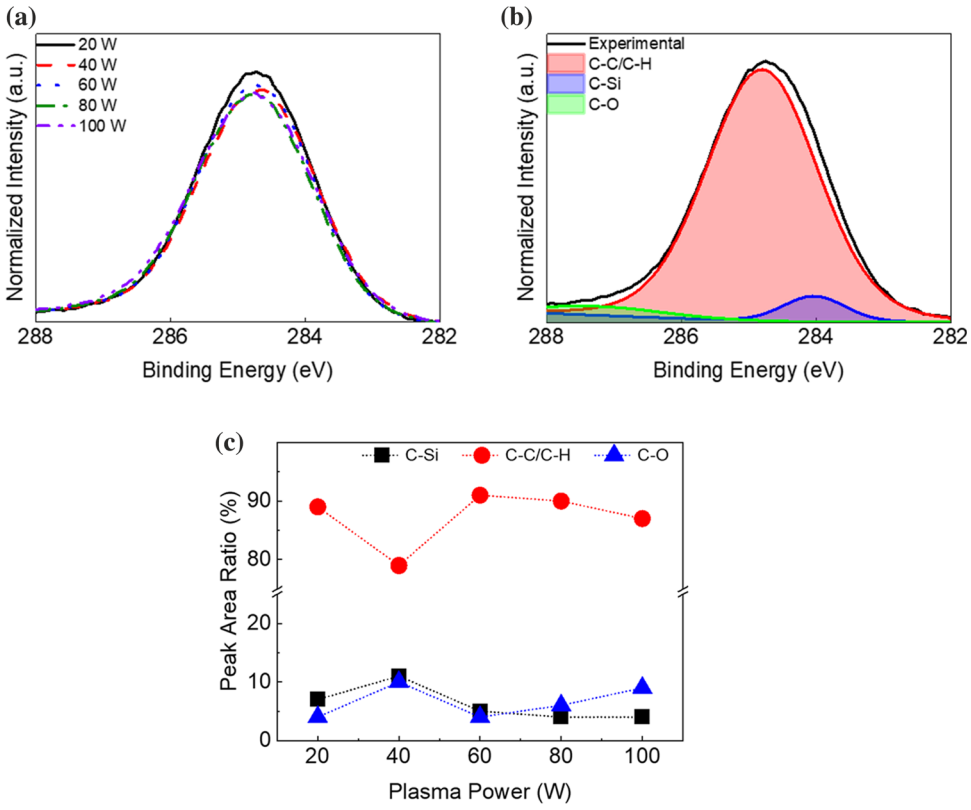

Figure 7 **a** XPS C1*s* peaks of the pristine flexible SiCOH films at various deposition plasma powers of 20–100 W, **b** deconvoluted C1*s* peak for 20 W, and **c** peak area ratios of silicon bonds at various plasma powers.

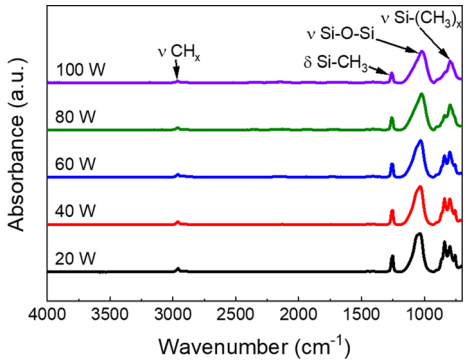

Figure 8 FTIR spectra of the pristine flexible SiCOH films at various deposition plasma powers of 20–100 W.

identify its constituent peaks. An example of the deconvoluted νSi–O–Si band for the film deposited at 20 W is shown in Fig. 9b. The deconvoluted peaks were identified as suboxide structure centered at 1025 cm^{-1}, network structure at 1065 cm^{-1}, and cage structure at 1115 cm^{-1} [18, 23, 24]. It is important to note that the cage structure is typically identified at 1135 cm^{-1}; however, the constituent peak identified at 1115 cm^{-1} is considered the cage structure of this film. This shift to lower wavenumbers indicated a smaller bond angle than 150° for Si–O–Si [23]. Network structure had a bond angle of 140° and suboxide had a bond angle lower than 140°. Figure 9c shows the peak area ratios of the cage, network, and suboxide to the total νSi–O–Si band of the SiCOH films at various deposition plasma powers. The peak area ratio of the cage structure was constant at 11% from 20 to 80 W and then slightly increased to 14% as the plasma power increased to 100 W. Increasing cage has been found to relate to increased porosity [23]. However, this contradicts the suggested increased density at higher deposition plasma powers found from the refractive index. The peak area ratio of the network structure decreased from 39 to 27% as the plasma power increased from 20 to 100 W. Suboxide structure had the largest peak area ratio, which increased from 49 to 60% as the plasma power increased from 20 to 100 W.

Figure 10a–c provides enlarged views of the νCH_x, $\delta Si–CH_3$, and $\nu Si–(CH_3)_x$ absorption bands, respectively. Table 1 shows peak area ratios of three absorption bands normalized to the Si–O–Si absorption band at various plasma powers. From a closer look at the νCH_x band, two possible bonds could be identified, the larger peak at 2960 cm^{-1} as ν^aCH_3 asymmetric stretching, and a smaller peak at 2902 cm^{-1} as ν^sCH_3 symmetric stretching. These

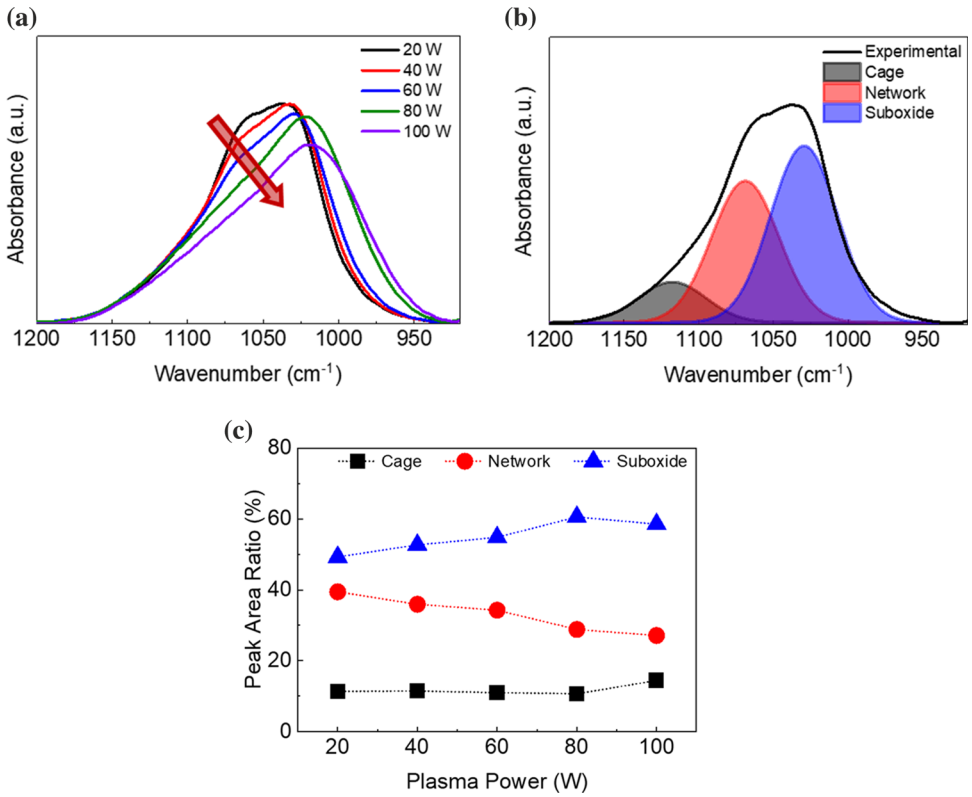

Figure 9 **a** FTIR spectra of the Si–O–Si absorption band of the pristine flexible SiCOH films at various deposition plasma powers, **b** deconvoluted Si–O–Si for 20 W, and **c** peak area ratios of the cage, network, and suboxide structures at various plasma powers.

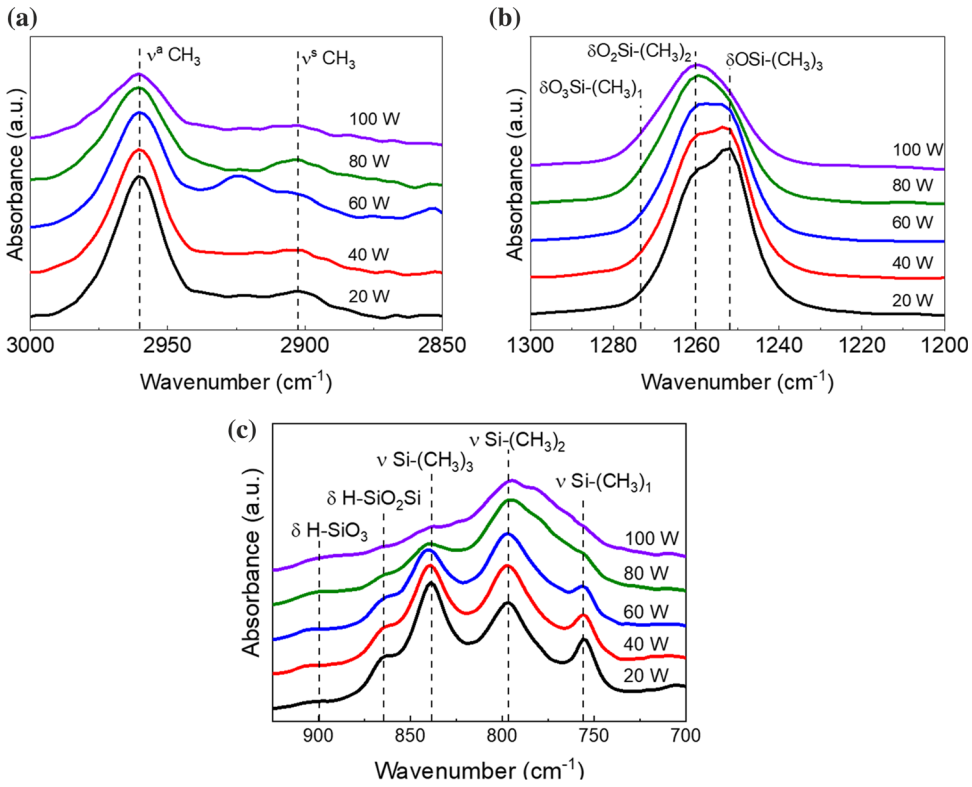

Figure 10 FTIR spectra of **a** νCH_x, **b** $\delta Si–CH_3$, and **c** $\nu Si–(CH_3)_x$ absorption bands of the pristine flexible SiCOH films at various deposition plasma powers.

Table 1 Peak area ratios of the FTIR absorption bands normalized to the Si–O–Si absorption band at various plasma powers

Plasma power (W)	Peak area ratios normalized to $\nu Si–O–Si$ (%)		
	νCH_x 2850–3000 cm^{-1}	$\delta Si–CH_3$ 1200–1300 cm^{-1}	$\nu Si–(CH_3)_x$ 650–950 cm^{-1}
20	3.6	10.1	73.3
40	3.1	9.3	67.8
60	4.0	8.8	64.8
80	2.5	7.7	59.2
100	1.7	6.8	56.7

bonds were formed from the methyl groups present in the SiCOH film. There was a decrease in intensity of the νCH_x band as the plasma power increased from 20 to 100 W. This indicated that the films contained less methyl groups when deposited at higher plasma powers. Previous studies have found that a reduction of the hydrophobic CH_3 can decrease the contact angle, thus making the film more hydrophilic [25]. This reduction of methyl groups at higher plasma powers could be the result of increased dissociation. Another possible bond identified for the film at 60 W only was ν^aCH_2 [20, 24]. This could result from the dissociation of C–H bonds in the TTMSS precursor. The νCH_x absorption band's peak area ratio was constant in the range of 3–4% up to 60 W and then decreased down to 1.7% at 100 W. This behavior also supported the deposition regime transition near 60 W and the reduction of methyl groups at higher plasma powers. The $\delta Si–CH_3$ absorption band was also found to slightly decrease in intensity as the plasma power increased from 20 to 100 W, indicating a decrease in methyl groups. There were three potential peaks that were identified as $\delta OSi–(CH_3)_3$ rocking at 1251 cm^{-1}, $\delta O_2Si–(CH_3)_2$ rocking at 1259 cm^{-1}, and $\delta O_3Si–CH_3$ rocking at 1279 cm^{-1}, assigned to M-, D-, and T-groups, respectively [18, 24]. These peaks refer to the number of O atoms bonded to a single Si atom. These are not

to be confused with the similar M-, D-, and T-groups found in the Si2*p* peak of the XPS spectra. As the plasma power increased from 20 to 100 W, the largest intensity peak shifted from 1251 to 1259 cm^{-1}, which indicated a preference for the D-group as the plasma power increased from 20 to 100 W. There was a significant decrease in the peak area ratio of Si–CH_3 from 10 to 6.8% as the plasma power increased from 20 to 100 W. This supported that there were fewer methyl groups at higher deposition plasma powers. From the νSi–$(CH_3)_x$ absorption band, the constituent peaks were identified as δH–SiO_3 bending at 890 cm^{-1}, δH–SiO_2Si bending at 864 cm^{-1}, νSi–$(CH_3)_3$ stretching at 839 cm^{-1}, νSi–$(CH_3)_2$ stretching at 796 cm^{-1}, and νSi–$(CH_3)_1$ stretching at 756 cm^{-1} [23, 24]. The highest intensity peak shifted from 839 to 796 cm^{-1}, indicating an increased νSi–$(CH_3)_2$ and a decreased νSi–$(CH_3)_3$ as the plasma power increased from 20 to 100 W. This further supported the reduced methyl groups in the SiCOH films at higher plasma powers. There was a decrease in intensity for νSi–$(CH_3)_3$, νSi–$(CH_3)_2$, and νSi–$(CH_3)_1$ as the plasma powers increased from 20 to 100 W, again suggesting reduced methyl groups at increased plasma power. Both δH–SiO_3 and δH–SiO_2Si were not significantly affected by the increased plasma power, suggesting that the Si–H bond was not significantly affected by the increased plasma power. The peak area ratios for the smaller absorption bands in Table 1 were identified as νSi–H (2150–2250 cm^{-1}) and δCH_x (1350–1500 cm^{-1}). The νSi–H absorption band was not observed for the film at 20 W and there was a slight increase from 0.4 to 2% as the plasma power increased from 40 to 100 W. It was reported that increased Si–H contributes to the hydrophilicity of the film [26]. The peak area ratio of δCH_x bending absorption band was almost the same for all deposition plasma powers, as seen in Table 1. It is expected that a reduction of methyl groups would decrease the peak area ratio of δCH_x as well. However, this is difficult to detect due to the small intensity of this peak.

Figure 11 presents dielectric constant of the pristine flexible SiCOH films at various deposition plasma powers of 20–100 W. The dielectric constants of the pristine SiCOH films for all plasma powers of 20–100 W were measured below 3.5, which can identify them as low-*k* materials. The dielectric constant decreased from 2.46 to 2.00 as the plasma power increased from 20 to 60 W, and then increased to 3.10

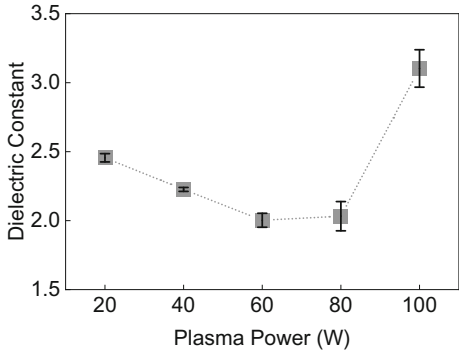

Figure 11 Dielectric constant of the pristine flexible SiCOH films at various deposition plasma powers of 20–100 W.

as the plasma power increased to 100 W. This behavior further supports the transition in deposition regimes. The dielectric constant can be related to the deposition rate (or the film thickness). Because the deposition time was fixed at 20 min for all samples, the trend of the deposition rate followed that of the thickness of the film. As the deposition rate (or the film thickness) increased with increasing plasma power from 20 to 60 W, the dielectric constant decreased. When the plasma power increased to 80 W, both deposition rate and dielectric constant did not change much. At the plasma power of 100 W, the deposition rate decreased and the dielectric constant increased. The decreased dielectric constant from 20 to 60 W could be explained by the increase in suboxide structure. However, the increased dielectric constant from 60 to 100 W could be explained by the methyl group reduction and increased density. As mentioned, the dielectric constant is affected by many chemical and physical properties of the SiCOH films.

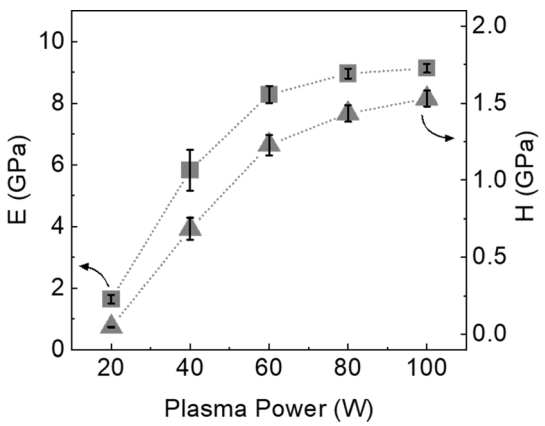

Figure 12 Elastic modulus and hardness of the pristine flexible SiCOH films at various deposition plasma powers of 20–100 W.

Figure 12 shows elastic modulus (E) and hardness (H) of the pristine flexible SiCOH films at various deposition plasma powers of 20–100 W. Both elastic modulus and hardness increased as the plasma power increased. The elastic modulus ranged from 1.6 to 9.1 GPa while the hardness ranged from 0.05 to 1.5 GPa when the plasma power increased from 20 to 100 W. For reference, the elastic modulus of 5–10 GPa is enough to sustain mechanical stress during typical semiconductor device integration. The film deposited at 20 W did not meet this criterion; however, the films deposited at the higher plasma powers above 20 W had sufficient elastic modulus. Both modulus and hardness had a greater slope below 60 W and a smaller slope above 60 W, again contributing to the possible transition in deposition regimes. As the deposition rate (or the film thickness) increased with increasing plasma power from 20 to 80 W, the elastic modulus and hardness increased. At the plasma power of 100 W, the deposition rate decreased and the modulus and hardness did not increase much.

The reduction of methyl groups could increase the dielectric constant [24, 27, 28]. Methyl groups are known to be hydrophobic, preventing water absorption. Water has a significantly higher dielectric constant ($k = \sim 81$). Therefore, even a relatively small amount of absorbed water can significantly affect the dielectric constant. However, there was no evidence of absorbed water for any of the pristine films. This would have been identified as O–H absorption band in the FTIR range of 3500–3800 cm^{-1}. In addition, there was only a slight decrease in contact angle, indicating no significant change in hydrophilicity from the reduction of methyl groups. This suggests that water absorption and hydrophilicity did not play a major role in the dielectric constant. The same can be suggested for the potential increase in Si–H bonds, which are known to be hydrophilic. However, methyl groups also affect the porosity of the film. It is known that the terminal structure of methyl groups aids the incorporation of pores [28, 29]. Porosity is known to decrease the dielectric constant, but also worsen the mechanical properties [27, 28, 30, 31]. For the low deposition plasma power regime, the increase in porosity explained the reduction in dielectric constant. However, it does not explain the increase in the elastic modulus and hardness. This may be explained by the suboxide structure. It has been reported that an increase in the suboxide structure results in a decrease in the dielectric constant [31, 32]. However, the suboxide structure improves the mechanical properties of the film [31–33]. Both the suboxide structure and the mechanical properties increased with increasing plasma powers. Two deposition regimes should be considered separately. The low plasma power deposition regime had a decreasing dielectric constant and increasing elastic modulus as the plasma power increased, while the higher plasma power deposition regime had both the dielectric constant and elastic modulus increasing as the plasma power increased. These regimes were possible because the increased suboxide effect was dominant for the dielectric constant in the lower power regime, while the methyl group reduction and increased density were dominant in the higher power regime. However, the increased suboxide and density could explain the increase in elastic modulus for both regimes.

It has been well documented that there is a correlation between the elastic modulus and the dielectric constant, where one increases and so does the other [30, 34–38]. To compare the results of this research to previous studies, a similar dielectric constant vs elastic modulus graph has been created as shown in Fig. 13. The data from this study followed this trend for the higher plasma power regime, deposited above 60 W. However, below 60 W this trend was not respected. It is hard to determine the reason for this disagreement for the films in the lower plasma power regime since SiCOH films have much variation with the bonding structure and porosity. However, the previous studies related the dielectric constant and elastic modulus to both the methyl group concentration and porosity of the film. This relationship was also found for the higher plasma power regime, where the decreased methyl groups and porosity

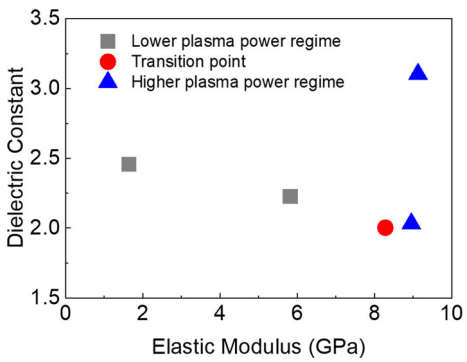

Figure 13 Dielectric constant and elastic modulus of the pristine flexible SiCOH films.

resulted in higher dielectric constant and elastic modulus. It is possible the previous research did not encounter the transition to the lower plasma power regime. Figure 13 is also be used to identify the optimum films for the IC integration. A lower dielectric constant and a higher elastic modulus can be found by moving down and to the right within this graph. The two data points in the lower right corner of the graph are the films deposited at 60 and 80 W. The film deposited at 60 W is defined as the transition point for the plasma power regimes, and 80 W is very close to this as well. This indicated that superior film properties are found when approaching the transition of the deposition regimes.

Repeated mechanical bending tests were conducted to investigate the effects of mechanical stress on material properties of flexible SiCOH thin films. Bending cycles were given by 1000, 5000, and 10,000. The SiCOH films deposited at 20, 60, and 100 W were selected for bending tests. The deposition plasma powers of 20, 60, and 100 W samples the lower plasma power regime, the transition point, and the higher plasma power regime, respectively.

Figure 14a–d shows the changes in refractive index, extinction coefficient, contact angle, and RMS roughness of the SiCOH films after bending tests, respectively. There was a slightly decreased refractive index for the films at 60 and 100 W. This could suggest that films deposited at the higher plasma power regime decreased in density after bending tests. However, the refractive index was not significantly changed even after bending with 10,000 cycles. The films experienced a slight decrease in extinction coefficient after bending tests. These films can still be considered transparent after bending because all extinction coefficients after bending tests were measured below 0.01. The contact angles of the films decreased after bending tests. This indicated that the films became slightly less hydrophobic after bending. Overall, the largest drop in the contact angle was observed for 100 W. For example, the contact angle for the film at 20 W decreased from 107.6° for the pristine film to 105.3°, 106.4°, and 107.6° after 1000, 5000, and 10,000 cycles, respectively. The film at 60 W experienced a decrease from 107.0 ° for the pristine film to 105.8°, 104.9°, and 106.0° after 1000, 5000, and 10,000 cycles, respectively. The film at 100 W experienced a decrease from 102.5° for the pristine film to 97.7°, 96.9°, and 99.7° after 1000, 5000, and 10,000 cycles, respectively. Overall, the SiCOH films maintained their hydrophobicity after bending tests. The roughness slightly increased for the film at 20 W, decreased for the film at 60 W, and stayed constant for the film at 100 W, except for 1000 cycles.

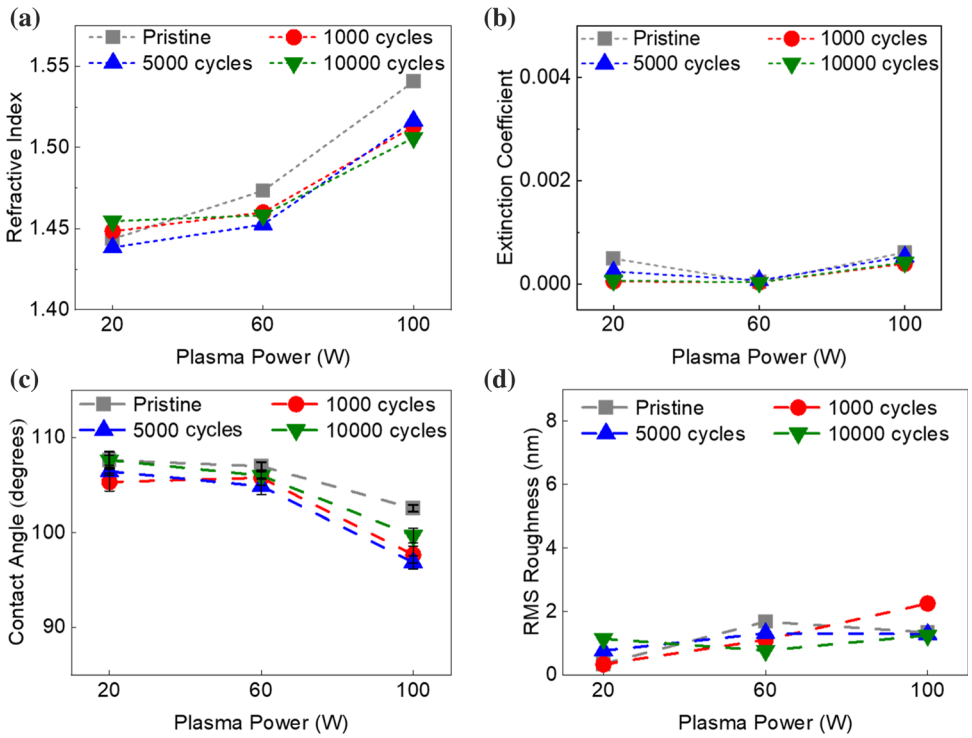

Figure 14 Changes in **a** refractive index, **b** extinction coefficient, **c** contact angle, and **d** RMS roughness of the flexible SiCOH films after bending tests.

Therefore, there is no evident trend between the surface roughness and bending conditions of the SiCOH films. However, all the films had a low roughness within 3 nm for all the bending conditions.

Figure 15a–d presents SEM images of the surface of the flexible SiCOH films at 20 W before and after bending tests with cycles of 1000, 5000, and 10,000, respectively. The images did not present any cracking or delamination at 500×magnification. SEM images were also taken with 5000×magnification, and no cracking or delamination was present, not shown here. The same was found for the films deposited at 60 and 100 W, not shown here. This indicated that the films were not damaged by the bending conditions even with 10,000 cycles. It demonstrated that the SiCOH films were mechanically stable after bending tests from observation using SEM.

FTIR spectra were taken to investigate the changes in chemical structures after bending tests. There were no significant changes in the spectra even after bending tests with 10,000 cycles. This suggested the flexible SiCOH films were chemically resistant to the repeated mechanical bending conditions. However, there were still some subtle changes after bending that can be seen upon closer inspection. Figure 16a–c shows FTIR absorption bands of the Si–O–Si for the flexible SiCOH films at 20, 60, and 100 W, respectively. The films at 20 W experienced a slight peak shift from 1038 cm^{-1} for the pristine film to a lower wavenumber of 1034 cm^{-1} after bending. The films at 60 W did not experience a shift after bending tests. There was a significant peak shift from 1020 to 1009 cm^{-1} for the films deposited at 100 W. This indicated that repeated mechanical bending may have promoted the suboxide structure, and this was even more pronounced for the higher plasma power regime. Figure 16d–f represents the changes in peak area ratios of cage, network, and suboxide structures normalized to the νSi–O–Si for the SiCOH films at 20, 60, and 100 W after bending tests, respectively. The peak area ratio of cage to νSi–O–Si of the film at 20 W was not significantly changed after bending tests. For the film at 60 W, the cage peak area ratio increased from 10.9% for the pristine film to 11.7% at 10,000 cycles. The film at 100 W experienced an increased cage peak area ratio from 14.4% for the pristine film to 16.0% after 5000 cycles and then decreased to 14.8% after 10,000 cycles. This indicated an increased cage peak area ratio after bending for the films deposited at the higher plasma power regime. For the film at 20 W, the network peak area ratio decreased from 39.4% for the pristine film to 37.8% after bending tests. There was a decrease in the network peak area ratio for the film at 60 W from 34.3% for the pristine film to 32.4% after 1000 cycles and then increased to 34.0% after 5000 and 10,000 cycles. The film at 100 W had an increased network peak area ratio from 27.1% for the pristine film to 31.0% after bending tests. This indicated that the films deposited

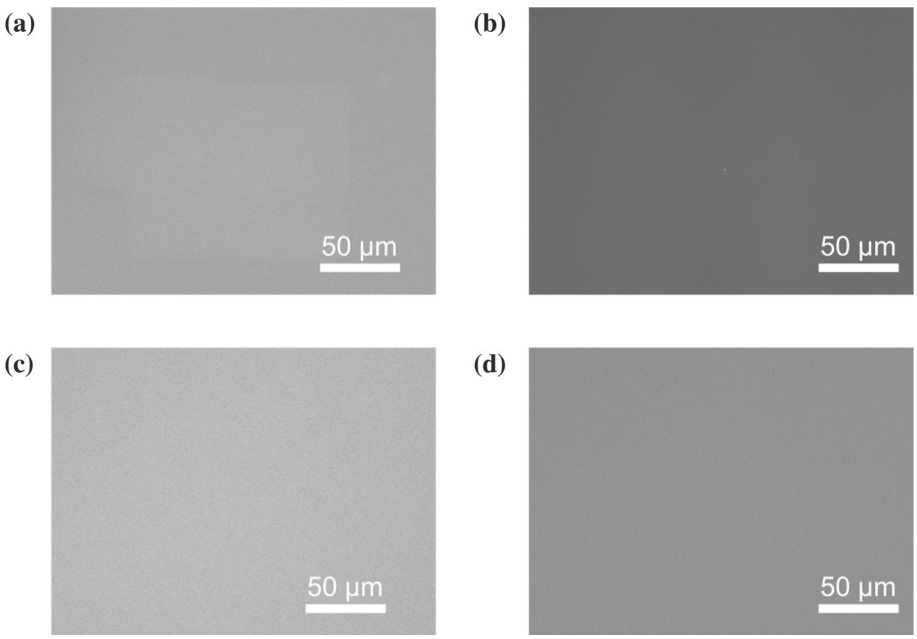

Figure 15 SEM surface images of **a** pristine SiCOH film deposited at 20 W and the films at 20 W after bending tests with bending cycles of **b** 1000, **c** 5000, and **d** 10,000.

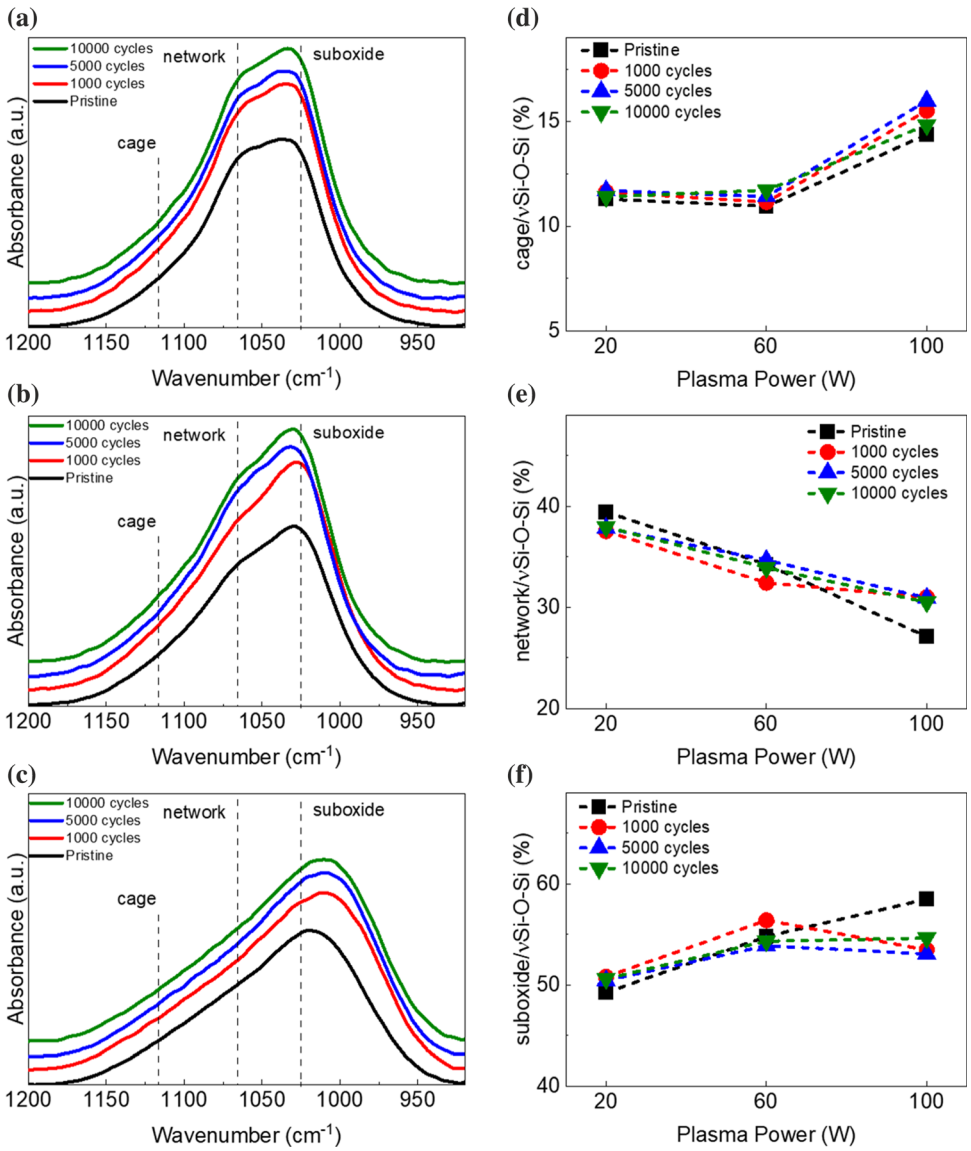

Figure 16 FTIR absorption bands of the Si–O–Si for the flexible SiCOH films at **a** 20, **b** 60, and **c** 100 W and changes in peak area ratios of **d** cage, **e** network, and **f** suboxide structures normalized to the Si–O–Si after bending tests.

at the higher plasma power regime increased in network structure, while the lower plasma power regime decreased in network structure. The suboxide peak area ratio slightly increased for the film at 20 W from 49.3% for the pristine film to 50.6% after bending tests. For the film at 60 W, the suboxide peak area ratio decreased from 54.8% for the pristine film to 53.9% at 5000 cycles and then increased to 54.4% at 10,000 cycles. For the film at 100 W, the suboxide peak area ratio significantly decreased from 58.5% for the pristine film to 53.1% at 5000 cycles and 54.6% at 10,000 cycles. This suggested that the higher plasma power regime significantly increased in the network structure and decreased in the suboxide structure. This is expected to slightly weaken the mechanical properties and increase the dielectric constant. The lower plasma power regime was slightly changed with a decreased network and increased suboxide structures. This suggested that the lower plasma power regime was more resistant to the repeated mechanical bending than the higher plasma power regime. However, a slight increase in mechanical properties and decrease in dielectric constant were expected. The film at 60 W was at the transition between the lower and higher plasma power regimes and proved to be the most chemically resistant to the repeated mechanical bending tests.

Figure 17a–c shows FTIR absorption bands of the νCH_x, $\delta Si–CH_3$, and $\nu Si–(CH_3)_x$ for the flexible SiCOH films at 20 W after bending tests, respectively.

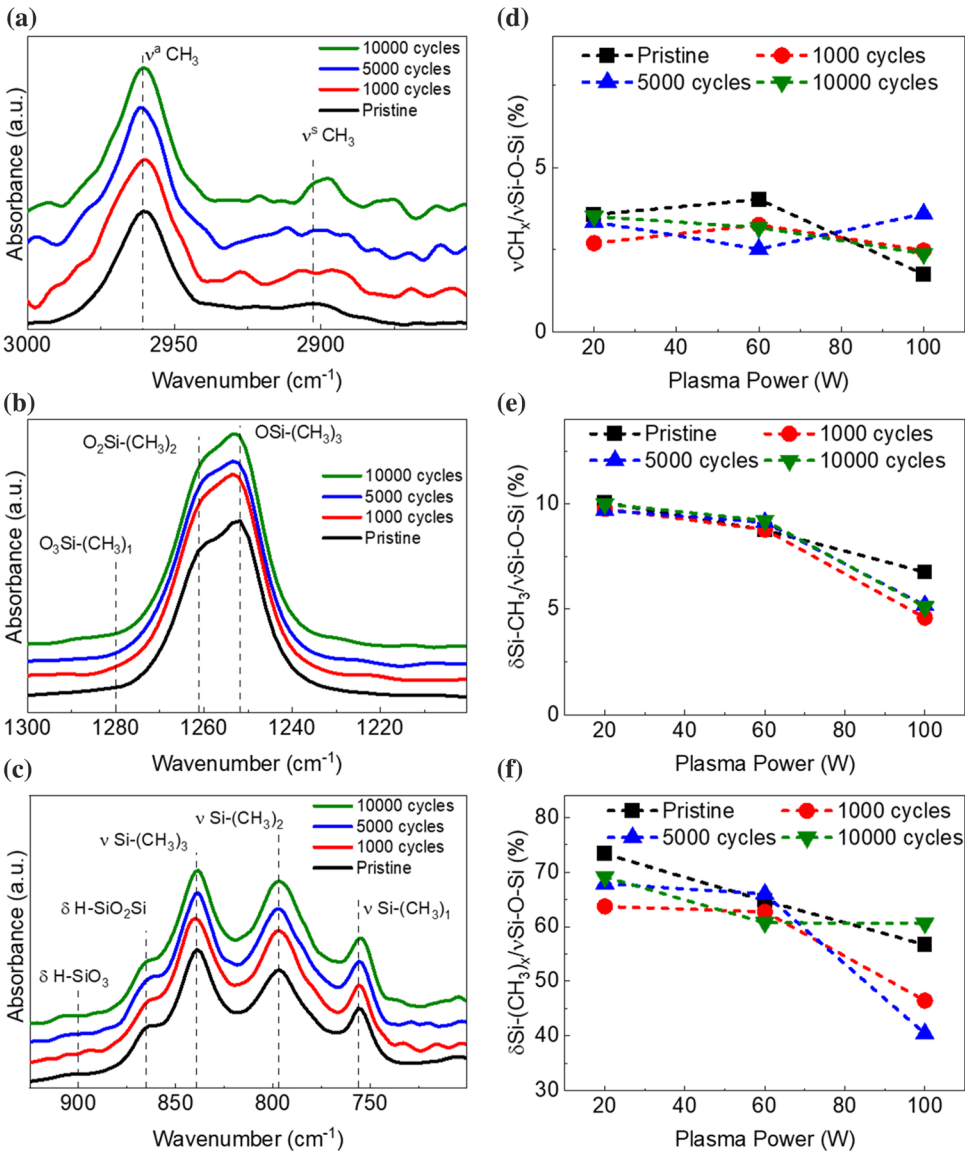

Figure 17 FTIR absorption bands of the **a** CH_x, **b** Si–CH_3, and **c** Si–$(CH_3)_x$ for the flexible SiCOH films at 20 W and changes in peak area ratios of **d** CH_x, **e** Si–CH_3, and **f** Si–$(CH_3)_x$ normalized to the Si–O–Si after bending tests.

For νCH_x peak, the larger ν^aCH_3 peak did not shift after bending tests. This indicated the asymmetric stretching CH_3 bond was resistant to the repeated mechanical bending tests. The ν^sCH_3 peak was very low in intensity, and it was therefore difficult to identify any peak center shifts, especially for the films deposited at 100 W (not shown). For the δSi–CH_3 peak, a slight peak shift to the higher wavenumbers occurred from 1252 to 1253 cm^{-1} for the film at 20 W after bending. The film at 60 W experienced no peak shift for 1000 cycles, but a peak shift occurred to lower wavenumbers from 1260 to 1255 cm^{-1} after 5000 and 10,000 cycles (not shown). The film at 100 W experienced a slight peak shift to higher wave numbers from 1260 to 1262 cm^{-1} after bending (not shown). For the νSi–$(CH_3)_x$ absorption band, there was no significant shift of the peak centers after bending for the films deposited at 20 W as well as 60 W (not shown). The film at 100 W experienced a peak shift from 795 to 790 cm^{-1} (not shown). This suggests that the νSi–$(CH_3)_1$ bond was slightly more resistant to the repeated mechanical bending than νSi–$(CH_3)_2$ for the films deposited at 100 W, even though νSi–$(CH_3)_2$ was still the highest intensity bond. The νSi–$(CH_3)_1$ bonding structure promotes more crosslinking than the νSi–$(CH_3)_2$ bonding structure. Therefore, a slight increase in mechanical strength was expected after bending tests for the films deposited at 100 W. Figure 17d–f presents the changes in peak area ratios of the νCH_x, δSi–CH_3, and

νSi–$(CH_3)_x$ normalized to the νSi–O–Si for the SiCOH films at 20, 60, and 100 W after bending tests, respectively. In the peak area ratios of the νCH_x normalized to νSi-O-Si for the films at 20 W, the ratio slightly decreased from 3.6% for the pristine film to 2.7% for 1000 cycles before it increased back to the pristine level for 5000 and 10,000 cycles. The films deposited at 60 W decreased from 4.0% for the pristine film to 3.2% at 1000 cycles and 2.5% for 5000 cycles before it increased back to 3.2% for 10,000 cycles. The film at 100 W showed an increase in the peak area ratio from 1.7% for the pristine film to 2.5% at 1000 cycles and 4.0% at 5000 cycles, then decreased again to 2.5% at 10,000 cycles. These results suggest that the film at 60 W had reduced methyl groups while the films at 100 W increased in methyl groups after bending. From the changes of peak area ratios of δSi–CH_3 to νSi–O–Si, bending had no significant effect on the peak area ratio for the films at 20 and 60 W. For the film at 100 W, there was a significant decrease in the peak area ratio of δSi–CH_3 to νSi–O–Si after bending. The peak area ratio decreased from 6.7% for the pristine film to 4.9% after bending. There was no trend with the number of bending cycles and the decrease in the peak area ratio. This indicates that the effect of bending on δSi–CH_3 occurred before 1000 cycles, and subsequent bending cycles had no significant effect. The δSi–CH_3 absorption band was stable for the film at 20 and 60 W, but not at 100 W. The decreased peak area ratio of δSi–CH_3 to νSi–O–Si indicates a reduction in methyl groups after bending. This suggests that the lower plasma power regime was more resistant to methyl group reduction from bending tests, as compared to the higher plasma power regime. This is contradictory to the results of the νCH_x absorption band after bending. The film at 100 W increased in the peak area ratio of νCH_x to νSi–O–Si but decreased in the peak area ratio of δSi–CH_3 to νSi–O–Si after bending tests. It is more likely that bending tests resulted in a decrease in methyl groups. This also agrees with the decreased contact angle after bending, resulting in a less hydrophobic film. From the changes in the peak area ratio of νSi–$(CH_3)_x$ to νSi–O–Si after bending, there was a decrease in the peak area ratio from 73% for the pristine film to 67% after bending for the film at 20 W. There is no trend between the number of bending cycles and the peak area ratio. The decreased peak area ratio of νSi–$(CH_3)_x$ to νSi–O–Si for the film at 20 W indicated a reduction of methyl groups. However, this was not observed in the νCH_x or the δSi–CH_3 peak area ratios for the film deposited at 20 W. For the film at 60 W, there was no significant change in the peak area ratio after bending tests. The films at 100 W experienced a decrease in the peak area ratio from 67% for the pristine film to 43% after 1000 and 5000 cycles, then increased to 61% after 10,000 cycles. There does not seem to be a consistent trend for the peak area ratio of the νSi–$(CH_3)_x$ to νSi–O–Si for the film at 100 W after bending. Overall, FTIR analysis did not uncover any consistent trends with the number of bending cycles. Therefore, the SiCOH films can be considered chemically stable to the bending conditions utilized in this research.

Figure 18 shows the changes in dielectric constant for the flexible SiCOH films deposited at the plasma powers of 20, 60, and 100 W after bending tests. The films deposited at 20 W experienced a slightly decreased dielectric constant from 2.46 for the pristine film to 2.31 at 1000 cycles, then it increased to 2.69 and 2.61 at 5000 and 10,000 cycles, respectively. For the film at 60 W, the dielectric constant decreased from 2.00 for the pristine film to 2.05 at 1000 cycles, 1.85 at 5000 cycles, and then increased to 1.97 at 10,000 cycles. For the film at 100 W, the dielectric constant decreased from 3.10 for the pristine film to 2.72. Overall, there was no significant effect on the dielectric constant from the repeated bending tests. The dielectric constant was not drastically affected by the repeated mechanical bending tests. More importantly, after bending tests, all dielectric constants remained below 3.5, which meets the requirement of low-*k* materials. There was no clear trend between the dielectric constant and bending cycles. Therefore, the repeated mechanical bending tests under the conditions utilized for this research had no observed

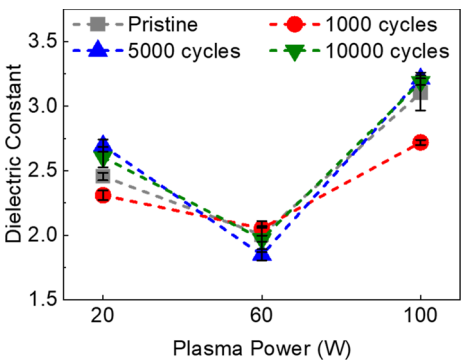

Figure 18 Changes in the dielectric constant for the flexible SiCOH films at 20, 60, and 100 W after bending tests.

effect on the dielectric constant. The film deposited at 60 W showed greater electrical stability to the repeated mechanical bending tests.

Conclusion

Flexible SiCOH films were deposited on flexible ITO/PEN substrates by PECVD of TTMSS at room temperature and various plasma powers of 20–100 W. All the pristine SiCOH films were transparent, hydrophobic, and smooth. These films also had dielectric constants below 3.5 and are considered low k materials. The films deposited at 40, 60, 80, and 100 W had sufficient mechanical strength for integration. For integration into IC chips, the films deposited at 60 and 80 W had the optimized properties of a very low dielectric constant $\sim$ 2.0 and high elastic modulus of 8–9 GPa. There was an increase in the suboxide structure, and film density in tandem with a reduction of methyl groups, as the plasma power increased. Two deposition regimes were observed and named as the lower and higher deposition power regimes. In the lower power regime, the dielectric constant decreased as the plasma power increased due to increased suboxide structure. For the higher plasma power regime, the dielectric constant increased as the plasma power increased due to methyl reduction and increased density. For both deposition regimes, the mechanical strength improved as the plasma power increased due to the increased suboxide structure and increased density. Subsequently, bending tests were performed on the flexible SiCOH films for the deposition plasma powers of 20, 60, and 100 W. After the bending tests, the flexible SiCOH films maintained their transparency, hydrophobicity, and smoothness. Low dielectric constant was maintained below 3.5 after bending tests. SEM imagery did not find any cracks or delamination of the flexible SiCOH films after bending tests. The flexible SiCOH films were physically, chemically, and electrically stable to the repeated mechanical bending tests with the conditions utilized in this research. However, the film deposited at 60 W proved to have better electrical and chemical stability when compared to the films at 20 and 100 W.

Acknowledgements

This work was supported by the National Science Foundation under Grant No. CMMI-2026801. The authors would like to thank the Nanofabrication Facility at Louisiana State University for use of nanofabrication equipment.

Declarations

Conflict of interest The authors declare that they have no conflict of interest. The authors declare that they have no known competing financial interests or personal relationships that could have appeared to influence the work reported in this paper.

Ethics approval Research results are not misrepresented. The results are presented clearly, honestly and without fabrication, falsification or inappropriate data manipulation. The results are appropriately placed in the context of prior and existing research. No data, text, or theories by others are presented as if they were the author's own. This is the authors' own original work, which has not been previously published elsewhere. The manuscript is not currently being considered for publication elsewhere. The manuscript reflects the authors' own research and analysis in a truthful and complete manner. The manuscript properly credits the meaningful contributions of co-authors. All authors have been personally and actively involved in substantial work leading to the manuscript and will take public responsibility for its content.

References

[1] Moore GE (1965) Cramming more components onto integrated circuits. Electronics 38:4

[2] Maex K, Baklanov MR, Shamiryan D, Lacopi F, Brongersma SH, Yanovitskaya ZS (2003) Low dielectric constant materials for microelectronics. J Appl Phys 93:8793–8841. https://doi.org/10.1063/1.1567460

[3] Baklanov M, Maex K, Green M (2007) Dielectric films for advanced microelectronics. John Wiley and Sons Ltd, West Sussex, England

[4] Grill A (2016) PECVD low and ultralow dielectric constant materials: from invention and research to products. J Vac Sci Technol 34:020801. https://doi.org/10.1116/1.4943049

[5] Grill A, Gates SM, Ryan TE, Nguyen SV, Priyadarshini D (2014) Progress in the development and understanding of

advanced low k and ultralow k dielectrics for very large-scale integrated interconnects-State of the art. Appl Phys Rev 1:011306. https://doi.org/10.1063/1.4861876

[6] Miyajima H, Ishikawa K, Sekine M, Hori M (2019) Review of methods for the mitigation of plasma-induced damage to low-dielectric-constant interlayer dielectrics used for semiconductor logic device interconnects. Plasma Process Polym 16:1900039. https://doi.org/10.1002/ppap.201900039

[7] Wang B, Huang W, Chi L, Al-Hashimi M, Marks TJ, Facchetti A (2018) High-k gate dielectrics for emerging flexible and stretchable electronics. Chem Rev 118:5690–5754. https://doi.org/10.1021/acs.chemrev.8b00045

[8] Hosseini MM, Nawrocki R (2021) A review of the progress of thin-film transistors and their technologies for flexible electronics. Micromachines 12:655. https://doi.org/10.3390/mi12060655

[9] Rogers JA, Bao Z, Baldwin K, Dodabalapur A, Crone B, Raju VR, Kuck V, Katz H, Amundson K, Ewing J, Drzaic P (2001) Paper-like electronic displays: large-area rubber-stamped plastic sheets of electronics and microencapsulated electrophoretic inks. Proc Natl Acad Sci 98:4835–4840. https://doi.org/10.1073/pnas.09158809

[10] Lee JK, Lim YS, Park CH, Park YI, Kim CD, Hwang YK (2010) a–Si: H thin-film transistor-driven flexible color E-paper display on flexible substrates. IEEE Electron Device Lett 31:833–835. https://doi.org/10.1109/LED.2010.2051531

[11] Na JW, Kim HJ, Hong S, Kim HJ (2018) Plasma polymerization enabled polymer/metal–oxide hybrid semiconductors for wearable electronics. ACS Appl Mater Interfaces 10:37207–37215. https://doi.org/10.1021/acsami.8b11094

[12] Li X, Li P, Wu Z, Luo D, Yu HY, Lu ZH (2021) Review and perspective of materials for flexible solar cells. Mater Rep Energy 1:100001. https://doi.org/10.1016/j.matre.2020.09.001

[13] Thompson AB, Woods DW (1956) The transitions of polyethylene terephthalate. Trans Faraday Soc 52:1383–1397. https://doi.org/10.1039/TF9565201383

[14] Hay J, Crawford B (2011) Measuring substrate-independent modulus of thin films. J Mater Res 26:727–738. https://doi.org/10.1557/jmr.2011.8

[15] You H, Mennell P, Shoudy M, Sil D, Dorman D, Cohen S, Liniger E, Shaw T, Leo T-L, Canaperi D, Raymond M, Madan A, Grill A (2018) Extreme-low k porous pSiCOH dielectrics prepared by PECVD. J Vac Sci Technol B 36:012202. https://doi.org/10.1116/1.5007177

[16] Inagaki N (2014) Plasma surface modification and plasma polymerization. CRC Press, Boca Raton. https://doi.org/10.1201/9781498710831

[17] Ding ZJ, Wang YP, Liu WJ, Ding SJ, Baklanov MR, Zhang DW (2018) Characterization of PECVD ultralow dielectric constant porous SiOCH films using triethoxymethylsilane precursor and cinene porogen. J Phys Appl Phys 51:115103. https://doi.org/10.1088/1361-6463/aaae79

[18] Park Y, Lim H, Kwon S, Ban W, Jang S, Jung D (2021) Ultralow dielectric constant SiCOH films by plasma enhanced chemical vapor deposition of decamethylcyclopentasiloxane and tetrakis (trimethylsilyloxy) silane precursors. Thin Solid Films 727:138680. https://doi.org/10.1016/j.tsf.2021.138680

[19] Chen G, Zhang J, Yang S (2008) Fabrication of hydrophobic fluorinated amorphous carbon thin films by an electrochemical route. Electrochem Commun 10:7–11. https://doi.org/10.1016/j.elecom.2007.10.006

[20] Kim CY, Jung AS, Navamathavan R, Choi CK (2008) Bonding configuration and electrical properties of carbon-incorporated low-dielectric-constant SiOC(-H) films with nano-pore structures deposited by using PECVD. J Korean Phys Soc 53:2621–2626. https://doi.org/10.3938/jkps.53.2621

[21] Jang H, Kim H, Lee S, Moon H, Jung D, Chae H (2017) Characterization of low-k SiCOH film etching in fluorocarbon inductively coupled plasmas. Nanosci Nanotechnol Lett 9:174–178. https://doi.org/10.1166/nnl.2017.2332

[22] Lee S, Woo J, Jung D, Yang J, Boo JH, Kim H, Chae H (2009) Effect of etching on dielectric constant and surface composition of SiCOH low-k films in inductively coupled fluorocarbon plasmas. Thin Solid Films 517:3942–3946. https://doi.org/10.1016/j.tsf.2009.01.104

[23] Grill A, Neumayer DA (2003) Structure of low dielectric constant to extreme low dielectric constant SiCOH films: fourier transform infrared spectroscopy characterization. J Appl Phys 94:6697–6707. https://doi.org/10.1063/1.1618358

[24] Lin Y, Tsui TY, Vlassak JJ (2006) Octamethylcyclotetrasiloxane-based, low-permittivity organosilicate coatings. J Electrochem Soc 153:F144. https://doi.org/10.1149/1.2202120

[25] Miyajima H, Masuda H, Watanabe K, Ishikawa K, Sekine M, Hori M (2019) Chemical bonding structure in porous SiOC films (k < 2.4) with high plasma-induced damage resistance. Micro Nano Eng 3:1–6. https://doi.org/10.1016/j.mne.2019.02.005

[26] Kubasch C, Olawumi T, Ruelke H, Mayer U, Bartha JW (2014) Investigation of argon plasma damage on ultra low-κ dielectrics. ECS J Solid State Sci Technol 4:N3023–N3028. https://doi.org/10.1149/2.0041501jss

[27] Grill A (2003) Plasma enhanced chemical vapor deposited SiCOH dielectrics: from low-k to extreme low-k

interconnect materials. J Appl Phys 93:1785–1790. https://doi.org/10.1063/1.1534628

[28] Lam JC, Tan H, Huang MY, Zhang F, Sun H, Shen Z, Mai Z (2012) Fourier transform infrared spectroscopy of low-k dielectric material on patterned wafers. Jpn J Appl Phys 51:111501. https://doi.org/10.1143/JJAP.51.111501

[29] Priyadarshini D, Nguyen SV, Shobha H (2017) Advanced single precursor based pSiCOH k = 2.4 for ULSI interconnects. J Vac Sci Technol B 35:021201. https://doi.org/10.1116/1.4974317

[30] O'Neill M, Haas MK, Peterson BK, Vrtis RN, Weigel SJ, Wu D, Bitner MD, Karwacki EJ (2005) Impact of pore size and morphology of porous organosilicate glasses on integrated circuit manufacturing. MRS Online Proc Libr 914:102. https://doi.org/10.1557/PROC-0914-F01-02

[31] Kikuchi Y, Wada A, Kurotori T, Sakamoto M, Nozawa T, Samukawa S (2013) Non-porous ultra-low-k SiOCH (k = 2.3) for damage-free integration and Cu diffusion barrier. J Phys Appl Phys 46:395203. https://doi.org/10.1088/0022-3727/46/39/395203

[32] Li H, Knaup JM, Kaxiras E, Vlassak JJ (2011) Stiffening of organosilicate glasses by organic cross-linking. Acta Mater 59:44–52. https://doi.org/10.1016/j.actamat.2010.08.015

[33] Sa YK, Bang J, Son J, Yu DY, Kim YC (2021) Enhanced thermos-mechanical reliability of ultralow-k dielectrics with self-organized molecular pores. Materials 14:2284. https://doi.org/10.3390/ma14092284

[34] Verdonck P, Wang C, Le QT, Souriau L, Vanstreels K, Krishtab M, Baklanov M (2014) Advanced PECVD SiCOH low-k films with low dielectric constant and/or high young's modulus. Microelectron Eng 120:225–229. https://doi.org/10.1016/j.mee.2013.10.028

[35] Kim H, Oh H, Lee C, Jung D, Boo J (2014) Characteristics of plasma polymerized low-dielectric constant SiCOH films deposited with tetrakis(trimethylsilyloxy)silane and cyclohexane precursors. Bull Korean Chem Soc 35:2941–2944. https://doi.org/10.5012/BKCS.2014.35.10.2941

[36] Urbanowicz AM, Vanstreels K, Verdonck P, Besien EV, Christos T, Shamiryan D, Gendtd SD, Baklanov MR (2011) Effect of UV wavelength on the hardening process of porogen-containing and porogen-free ultralow-k plasma-enhanced chemical vapor deposition dielectrics. J Vac Sci Technol B 29:032201. https://doi.org/10.1116/1.3572063

[37] Kwon S, Ban W, Kim H, Park Y, Kim Y, Yu S, Jung D (2018) Single precursor based ultra-low k thin film deposited with tetrakis(trimethylsilyloxy)silane in PECVD system. Sci Adv Mater 10:1147–1153. https://doi.org/10.1166/sam.2018.3292

[38] Comeaux J, Wirth W, Courville J, Baek NW, Jung D, Jang S (2022) Etching characteristics of low-k SiCOH thin films under fluorocarbon-based plasmas. Vacuum 202:111165. https://doi.org/10.1016/j.vacuum.2022.111165